Molecular Therapy
Nucleic Acids
Original Article

Positive feedback loop of miR-320 and CD36 regulates the hyperglycemic memory-induced diabetic diastolic cardiac dysfunction

Jiabing Zhan,[1,2,3] Kunying Jin,[1,2,3] Nan Ding,[1,2] Yufei Zhou,[1,2] Guo Hu,[1,2] Shuai Yuan,[1,2] Rong Xie,[1,2] Zheng Wen,[1,2] Chen Chen,[1,2] Huaping Li,[1,2] and Dao Wen Wang[1,2]

[1]Division of Cardiology, Tongji Hospital, Tongji Medical College, Huazhong University of Science and Technology, Wuhan 430030, China; [2]Hubei Key Laboratory of Genetics and Molecular Mechanisms of Cardiological Disorders, Wuhan 430030, China

Intensive glycemic control is insufficient for reducing the risk of heart failure among patients with diabetes mellitus (DM). While the "hyperglycemic memory" phenomenon is well documented, little is known about its underlying mechanisms. In this study, a type 1 DM model was established in C57BL/6 mice using streptozotocin (STZ). Leptin receptor-deficient (db/db) mice were used as a model of type 2 DM. A type 9 adeno-associated virus was used to overexpress or knock down miR-320 *in vivo*. Diastolic dysfunction was observed in the type 1 DM mice with elevated miR-320 expression. However, glycemic control using insulin failed to reverse diastolic dysfunction. miR-320 knockdown protected against STZ-induced diastolic dysfunction. Similar results were observed in the type 2 DM mice. *In vitro*, we found that miR-320 promoted CD36 expression, which in turn induced further miR-320 expression. CD36 was rapidly induced by hyperglycemia at protein level compared with the much slower induction of miR-320, suggesting a positive feedback loop of CD36/miR-320 with CD36 protein induction as the initial triggering event. In conclusion, in DM-induced cardiac injury, miR-320 and CD36 mutually enhance each other's expression, leading to a positive feedback loop and a sustained hyperlipidemic state in the heart.

INTRODUCTION

The global diabetes prevalence in 2019 was estimated to be 9.3% (463 million people) and is expected to rise to 10.2% (578 million) by 2030 and 10.9% (700 million) by 2045.[1] Patients with diabetes mellitus (DM) have a high risk of developing heart failure, even after adjusting for coronary artery disease or hypertension. This has led to the increased recognition of a distinct disease process defined as diabetic cardiomyopathy (DCMP).[2,3] The onset and progression of DCMP are complex and involve early diastolic dysfunction, cardiac hypertrophy, ventricular dilation, and systolic dysfunction. They can occur independent of a recognizable cause, such as myocardial ischemia.[4] Left ventricular diastolic dysfunction is one of the first signs of DCMP prior to the development of irreversible systolic dysfunction.[5] Clinically, heart failure with preserved ejection fraction (HFpEF), characterized by diastolic dysfunction, may also present as an early stage of DCMP, reinforcing the importance of mechanistic investigation and the critical need for effective intervention.[6,7]

Pathological mechanisms that contribute to DCMP include metabolic disturbances, insulin resistance, formation, and crosslinking of advanced glycation end-products, mitochondrial damage, oxidative stress, inflammation, and cell death.[8,9] Hyperglycemia is regarded as a causal event in diabetes-induced cardiac dysfunction. However, most clinical trials focusing on intensive blood glucose control have achieved very limited success in cardiac protection,[10] which indicates that transient hyperglycemia might exert long-lasting heart damage, even after blood glucose levels return to normal. This phenomenon is referred to as "hyperglycemic" or "metabolic" memory.[11] Although the hyperglycemic memory phenomenon is well established, the underlying molecular mechanisms remain largely unknown.[12]

MicroRNAs (miRNAs) are short RNA molecules that are 19–25 nucleotides in size and regulate the post-transcriptional silencing of target genes.[13] A single miRNA can target hundreds of mRNAs and influence the expression of multiple genes often involved in a functionally related pathway.[14] Numerous cardiac miRNAs are crucial modulators of various cardiovascular diseases such as heart failure and DCMP.[4,15,16] At the cellular level, miRNA-targeted genes are involved in multiple pathophysiological processes critical for cardiac

Received 1 June 2022; accepted 12 December 2022;
https://doi.org/10.1016/j.omtn.2022.12.009.

[3]These authors contributed equally

Correspondence: Dao Wen Wang, Division of Cardiology, Tongji Hospital, Tongji Medical College, Huazhong University of Science and Technology, 1095# Jiefang Ave., Wuhan 430030, China.
E-mail: dwwang@tjh.tjmu.edu.cn
Correspondence: Huaping Li, Division of Cardiology, Tongji Hospital, Tongji Medical College, Huazhong University of Science and Technology, 1095# Jiefang Ave., Wuhan 430030, China.
E-mail: huapingli_tj@126.com
Correspondence: Chen Chen, Division of Cardiology, Tongji Hospital, Tongji Medical College, Huazhong University of Science & Technology, 1095# Jiefang Ave., Wuhan 430030, China.
E-mail: chenchen@tjh.tjmu.edu.cn

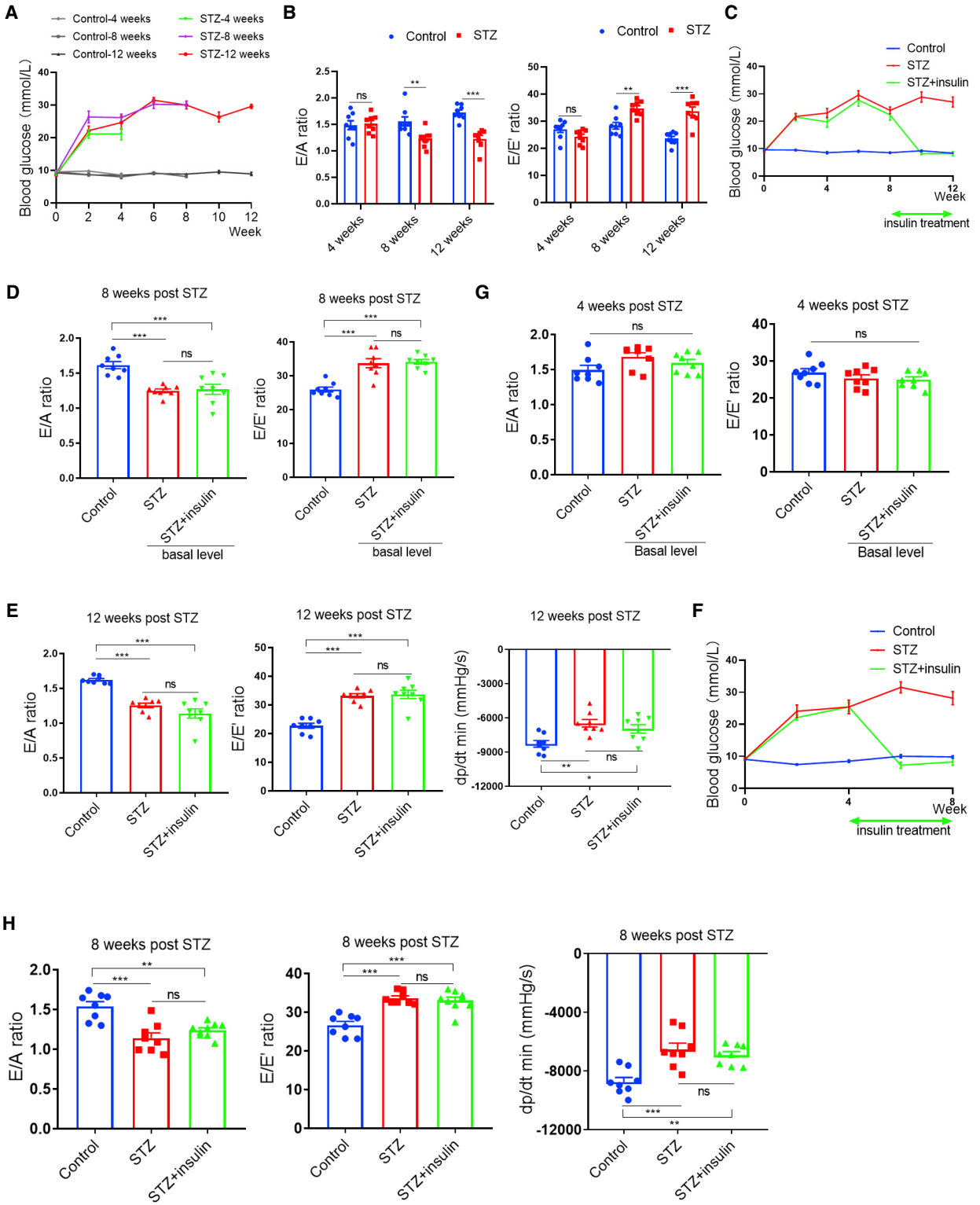

(legend on next page)

remodeling such as mitochondrial homeostasis, reactive oxygen species (ROS) generation, Ca^{2+} perturbation, apoptosis, fibrosis, and neurohormone secretion.[17–19] A recent study identified 316 dysregulated miRNAs in the hearts of streptozotocin-induced DM mice.[3] Glycemic control could not rescue the expression pattern of certain hyperglycemia-induced miRNAs in the diabetic heart.[3] This raised the question of the potential role of miRNAs in the pathogenesis of DCMP after blood glucose level normalization.

In previous studies, we investigated the functional properties of several subcellular localized miRNAs in various cardiovascular diseases[20–25] and found that cytoplasmic miR-21 protects against DCMP-induced diastolic dysfunction by targeting gelsolin.[22] Overexpression of cytoplasmic miR-30c represses BECN1 expression and improves cardiac function in diabetic mice.[23] Additionally, mitochondria-targeted miR-21 lowers blood pressure in spontaneously hypertensive rats by upregulating mitochondrial translation.[26] Finally, nuclear miR-320 contributes to diabetes-induced cardiac dysfunction by activating the transcription of the fatty acid (FA) metabolic gene CD36, leading to lipotoxicity in the heart.[27]

While miR-320 is a CD36 transcriptional activator, unexpectedly, the cardiac CD36 overexpression seems to increase miR-320 expression in turn,[27] implying that miR-320 and CD36 might form a positive feedback loop. In the current study, we attempted to determine whether this feedback loop really exists and its role in HFpEF, the early and irreversible DCMP stage. Our results showed that miR-320 promoted CD36 expression, and in turn, CD36 was able to increase miR-320 expression. This vicious cycle led to sustained elevation of free fatty acid (FFA) uptake and myocardial lipotoxicity even after normalization of hyperglycemia.

RESULTS

Glycemic control using insulin could not rescue streptozotocin-induced diabetic diastolic dysfunction

To confirm the presence of hyperglycemic memory in the animal models, we first analyzed the temporal pattern of hyperglycemic effect on cardiac performance (Figure S1A). Streptozotocin (STZ) treatment steadily increased the circulating glucose levels in C57BL/6J mice (Figures 1A and S2A). Cardiac performance was evaluated using echocardiography at 4, 8, and 12 weeks after STZ treatment, respectively. Although the systolic function remained normal during the observation period, analysis of E/A and E/E′ ratios showed clear diastolic dysfunction 8 weeks after hyperglycemic episode (Figures 1B and S2B, Table S1).

Subsequently, we investigated whether glycemic control using insulin could rescue or prevent the occurrence and progression of diastolic cardiac dysfunction in STZ-induced diabetic mice. Clinically, insulin remains the fundamental treatment for both type 1 DM (T1DM) and type 2 DM (T2DM) patients, especially for those with very high levels of glucose, and oral hypoglycemic agents are less effective. Therefore, in this study, insulin was selected for glycemic control instead of other hypoglycemic agents. Hyperglycemia was induced by STZ for 8 weeks, followed by 4 weeks of insulin treatment (Figures 1C, S1B, and S2C). As shown in Figures 1D and 1E, compared with the non-insulin treated mice, the diastolic function at the end of experimental period did not improve with insulin (Figures 1D, 1E, and S2D), indicating that glycemic control by insulin was unable to reverse the established diastolic dysfunction in the diabetic model. Systolic function remained unaltered in the three experimental groups (Tables S2 and S3, Figures S2E and S2F).

We then explored whether insulin could prevent the onset of diastolic dysfunction (Figures 1F, S1C, and S2G). Insulin treatment was initiated 4 weeks after STZ treatment when diastolic function was still normal (Figures 1G, S2H, and S2I, Table S4). However, in mice that were administered insulin 4 weeks earlier, diastolic dysfunction still occurred 8 weeks after STZ treatment (Figures 1H and S2H–S2J, Table S5).

These findings suggested that after 4 weeks of hyperglycemic stress, insulin treatment was no longer able to prevent or reverse diastolic dysfunction, indicating that hyperglycemia memory has been established 4 weeks after the hyperglycemic stress.

miR-320 knockdown protected against STZ-induced diastolic dysfunction

Glycemic control is unable to completely restore the hyperglycemia-induced miRNA landscape alterations to normal levels in the diabetic heart.[3] We speculated that hyperglycemic memory in diabetic hearts might be mediated by specific miRNAs. By reviewing data from previously published studies, three miRNAs (miR-34, miR-320, and miR-221) were identified as hyperglycemia-related miRNAs out of the candidate miRNAs.[3,23,27–32] These three miRNAs were dysregulated not only in both human and mouse diabetic hearts, but also in both type 1 and type 2 diabetic hearts (Figure 2A). The expression of these three miRNAs was measured in the heart of STZ-induced diabetic mice; miR-320 was the most abundant (Figure 2B). Consistent with a previous report,[3] the induced miR-320 expression in the

Figure 1. Glycemic control by insulin was unable to rescue STZ-induced diabetic diastolic dysfunction

(A) Time course analysis of blood glucose levels in random-fed state 4, 8 , and 12 weeks after STZ treatment, respectively. N = 8. (B) Echocardiographic analysis of E/A ratio and E/E′ ratio in STZ-induced diabetic mice after 4, 8, and 12 weeks of hyperglycemia, respectively. N = 8. (C) Time course analysis of blood glucose levels in random-fed state in control, STZ, and STZ + insulin treatment groups for 12 weeks. N = 8. (D) Echocardiographic analysis of E/A ratio and E/E′ ratio 8 weeks after STZ treatment prior to glycemic control by insulin. dp/dt min: peak instantaneous rate of LV pressure decrease. N = 8. (E) Echocardiographic and hemodynamic analysis of diastolic function markers 12 weeks after STZ treatment with 4 weeks glycemic control by insulin. N = 8. (F) Time course analysis of blood glucose levels in random-fed state in control, STZ, and STZ + insulin treatment groups for 8 weeks. N = 8. (G) Echocardiographic analysis of E/A ratio and E/E′ ratio 4 weeks after STZ treatment prior to glycemic control by insulin. N = 8. (H) Echocardiographic and hemodynamic analysis of diastolic function markers 8 weeks after STZ treatment with 4 weeks glycemic control by insulin. N = 8. (A)–(H) *p < 0.05, **p < 0.01, ***p < 0.001; (B) Student's t test; (D), (E), (G), and (H) one-way ANOVA.

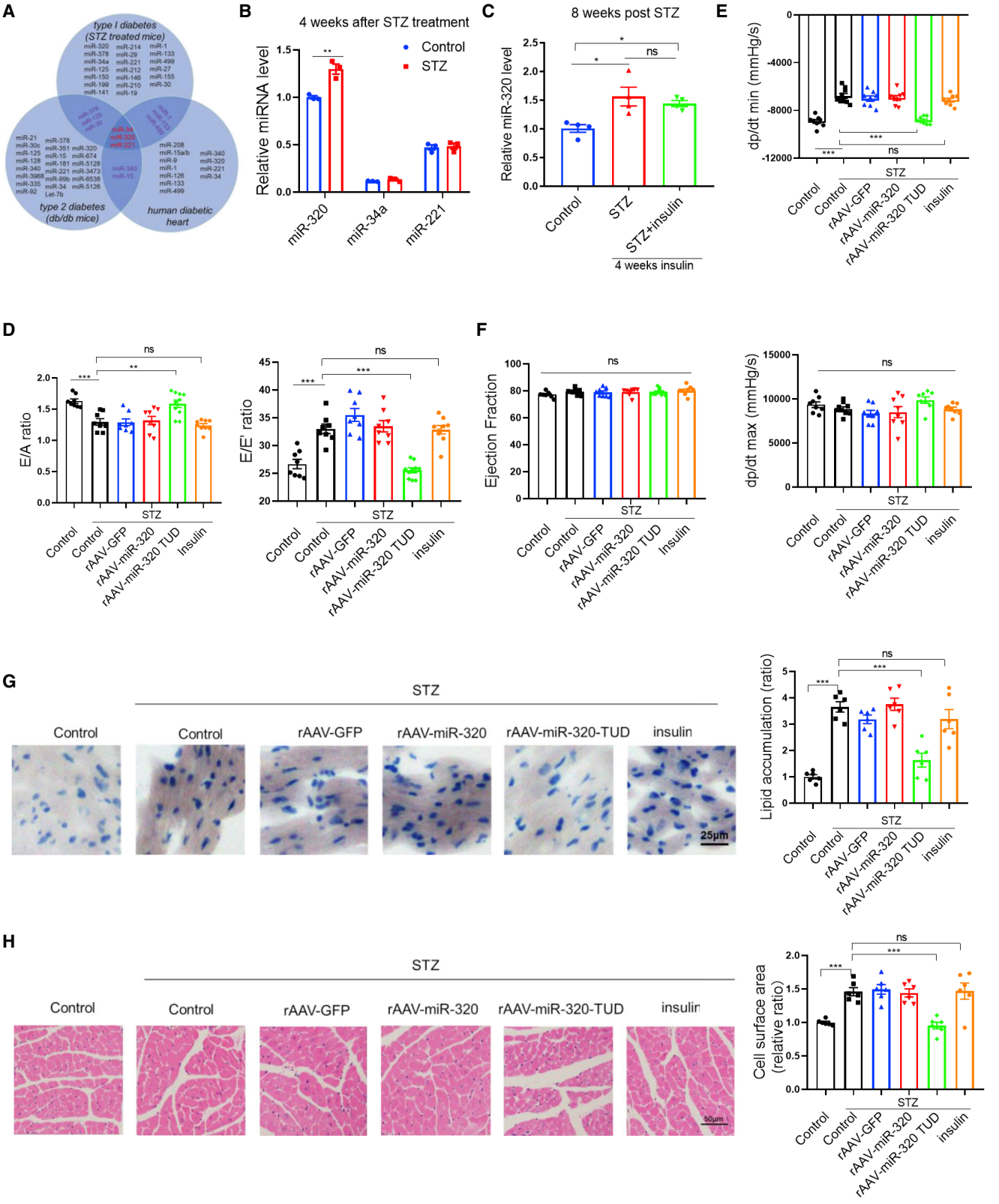

(legend on next page)

diabetic heart was not normalized by insulin treatment (Figure 2C). Moreover, miR-320 was increased in cardiomyocytes (CMs) but not in non-CMs in the STZ-induced mice (Figures S3A and S3B). These features prompted us to further investigate miR-320's role in hyperglycemic memory in the pathogenesis of DCMP.

Using the recombinant adeno-associated virus (rAAV, type 9) system, an miR-320 mimic or inhibitor designed with a tough decoy structure (TUD) was delivered into the mouse heart. Four weeks after STZ treatment, when the diastolic dysfunction was still normal, insulin pump and different AAVs were delivered, including rAAV-miR-320, rAAV-miR-320 TUD, and rAAV-green fluorescent protein (GFP) (Figures S1D and S3C). After an additional 4 weeks, the mice treated with rAAV-miR-320 TUD showed improved diastolic function compared with the STZ controls; the mice treated with insulin did not (Figures 2D and 2E). No significant changes in the systolic function were detected between the experimental groups (Figure 2F, Table S6). Consistent with our previous findings,[27] STZ-induced lipid accumulation in cardiomyocytes and cardiac hypertrophy was attenuated by rAAV-miR-320 TUD administration (Figures 2G and 2H). However, interstitial fibrosis was not affected by either miR-320 TUD or miR-320 AAV treatment (Figure S3F). rAAV-miR-320 overexpression did not show any detectable effects on cardiac function (Figures 2D–2F, Table S6; see details in discussion section).

miR-320 knockdown protected against diastolic dysfunction in db/db mice

We used db/db mice, a well-established rodent model for T2DM and its complications, to investigate the role of miR-320 in hyperglycemic memory. The detailed animal process is presented in the supplemental information (Figures S1E and S4A). Similar to STZ-induced T1DM, insulin treatment decreased the blood glucose levels in db/db mice but failed to reverse the increase in miR-320 levels and diastolic dysfunction (Figures 3A–3C, Table S7). In contrast, miR-320 TUD treatment improved cardiac diastolic function, reduced cardiac lipid accumulation, and attenuated cardiac hypertrophy in db/db mice (Figures 3B–3F). miR-320 TUD had no significant effect on interstitial fibrosis in db/db mice (Figure S4D).

These findings suggested that while glycemic control by insulin failed, miR-320 inhibition protected against diastolic dysfunction in both T1DM and T2DM mouse models.

CD36/miR-320 positive feedback loop in cardiomyocytes

CD36 is a key downstream target gene of miR-320-mediated transcriptional activation in the nucleus.[27] However, the mechanisms underlying miR-320 upregulation in DCMP remain unknown. Cardiac CD36 overexpression increased the expression of miR-320 *in vivo*,[27] implying that miR-320 and CD36 might form a positive feedback loop. In this study, CD36 overexpression indeed increased miR-320 expression, whereas CD36 knockdown decreased miR-320 levels in cultured cardiomyocytes (Figures 4A and 4B).

To illustrate the specific molecular mechanism of CD36-mediated miR-320 activation, we screened the potential transcription factors (TFs) that could directly enhance miR-320 transcription using the JASPAR (JASPAR CORE vertebrates collection [2022])[33] and TRANSFAC 2.0 database. SP1, GATA4, C-MYC, SMAD, and RXR were identified as potential factors that can target the promoter regions of miR-320 in humans, mice, and rats. Only SP1 levels significantly increased in our study after high-glucose treatment in cardiomyocytes (Figure 4C). *In vivo* analysis showed that SP1 expression increased in the STZ and db/db models (Figures S5A–S5C). Moreover, SP1 expression increased miR-320 expression in cardiomyocytes (Figure 4D), which is in line with previous observations in the endothelial cell.[24] CD36 overexpression also increased SP1 expression (Figure 4E). Thus, CD36 increases miR-320 expression by activating SP1. Furthermore, we observed that CD36-induced miR-320 expression was abolished by SP1 knockdown (Figures 4F and 4G), indicating that the CD36 regulation of miR-320 was SP1 dependent.

Next, we investigated the mechanism by which CD36 increases SP1 expression. CD36 can accelerate ROS generation in macrophages.[34] ROS activates SP1 through the PKC/MAKP pathway in tubular epithelial cells.[35] We attempted to determine whether the CD36-ROS-SP1 axis also exists in myocytes. We found that CD36-mediated activation of SP1 expression was abolished by the ROS scavenger N-acetylcysteine (NAC) in myocytes (Figure 4H).

We observed an increase in cardiac miR-320 and CD36 protein levels 8 weeks after STZ treatment *in vivo*. Moreover, this increase was not abolished by 4 weeks of glycemic control using insulin (Figures 2C and 4I). A similar result was also observed in T2DM db/db mice (Figure S4E). These data indicated the presence of a CD36/miR-320 positive feedback loop in hyperglycemic myocytes (Figure 4J). Consistent with this schematic diagram, we found that SP1 was able to regulate CD36 expression under prolonged treatment conditions when miR-320 was pre-modulated by SP1 in advance (Figures S5D and S5E). A feedback loop of miR-320 and CD36 was also observed in primary neonatal rat ventricular myocytes (Figures S6A and S6B).

Figure 2. miR-320 knockdown protected against diastolic dysfunction induced by STZ treatment

(A) Strategy for identifying diabetes-related miRNAs in human and animal models. (B) Quantitative real-time PCR analysis of miR-320, miR-34a, and miR-221 levels in diabetic heart 4 weeks after STZ treatment in comparison with controls. N = 4. (C) Quantitative real-time PCR analysis of miR-320 levels in the heart from control, diabetes without glycemic control, and diabetes with glycemic control groups. N = 4. (D)–(F) Echocardiographic and hemodynamic analysis in different groups. dp/dt max and dp/dt min, peak instantaneous rate of LV pressure increase and decrease, respectively. N = 8–10. (G) Cardiac lipid deposition detected by oil red staining in different groups. N = 5–6. (H) Cardiomyocytes visualization and size quantitation by H&E staining in different groups. N = 5–6. (A)–(H) *$p < 0.05$, **$p < 0.01$, ***$p < 0.001$; (B) Student's t test; (C)–(H) one-way ANOVA.

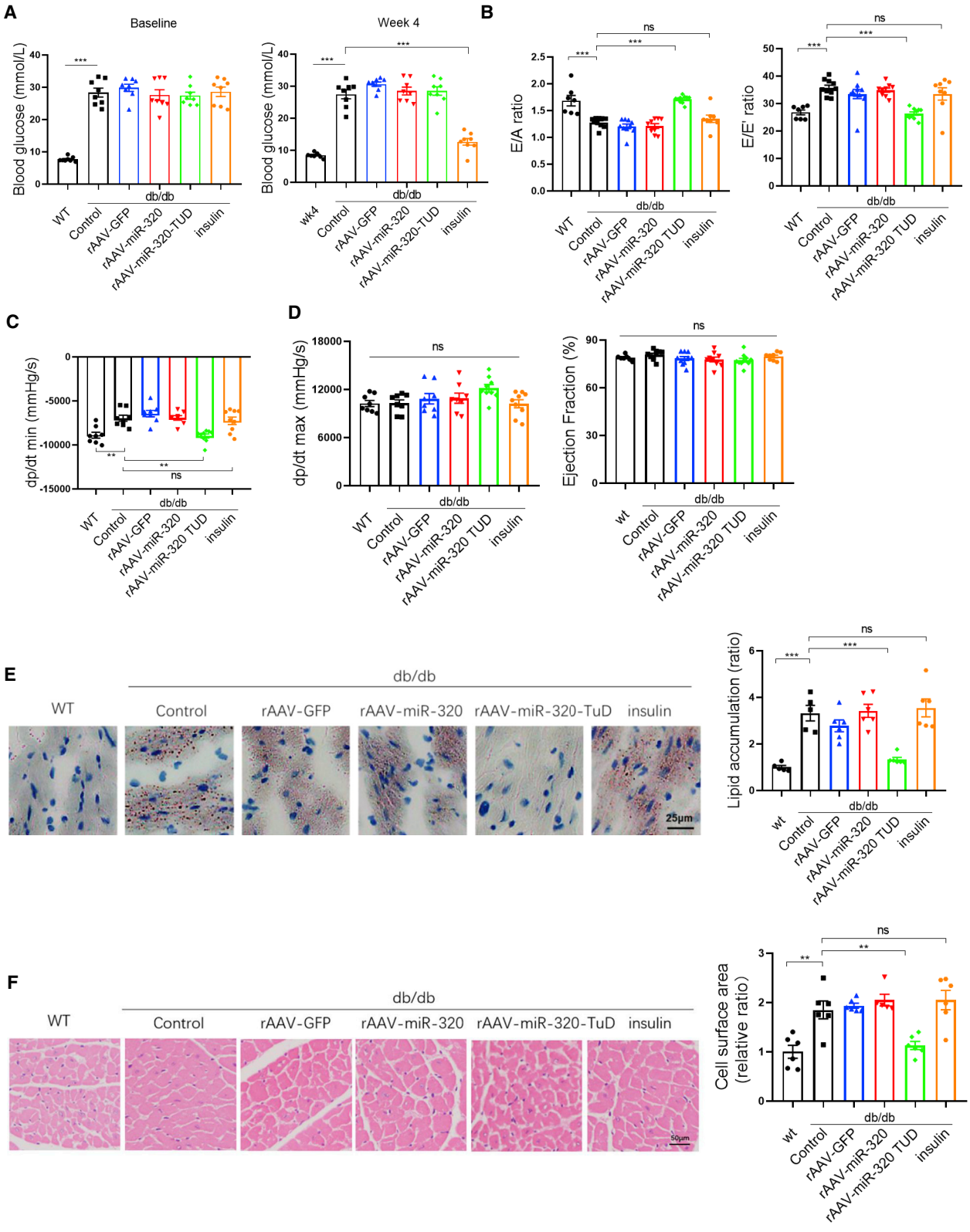

(legend on next page)

CD36 induction initiated the CD36/miR-320 feedback loop during the early hyperglycemic stage

Next, we attempted to identify the initial trigger in the CD36/miR-320 positive feedback loop. Time course analysis of CD36 and miR-320 expression in the heart of STZ-treated mice indicated that CD36 upregulation preceded the increase in miR-320 (Figures 5A and 5B). Specifically, CD36 significantly increased 2 weeks after the hyperglycemic induction, whereas an miR-320 increase was observed only after 4 weeks of STZ administration (Figures 5A and 5B). This suggested that CD36 induction may be the initial trigger in the CD36/miR-320 positive feedback loop. However, we noted that 2 weeks after the hyperglycemic induction, the CD36 mRNA level did not increase, indicating that the CD36 protein upregulation at 2 weeks after STZ administration was achieved by post-transcriptional regulation (Figure 5C). *In vitro*, high-glucose treatment rapidly induced CD36 protein expression as early as within 6 h of treatment, but it did not affect CD36 mRNA expression until 48 h later (Figures 5D and 5E). To further investigate how high-glucose stress induced CD36 expression in the early stage, we performed polysome profiling analysis, which is the gold standard for studying translational regulation in AC-16 cells. We detected small and large ribosome fractions, as well as monosomes, on a 10%–50% sucrose gradient, which was characterized by 18S and 28S rRNAs distribution and representative ribosomal proteins (RPS3 and RPL4) in the expected fractions (Figure 5F). We also detected potential polysome fractions near the bottom of the gradient (fractions 11 and 12) that could be converted to monosomes by RNase I treatment (Figure 5F). By quantitative real-time PCR quantification of CD36 mRNA and plotting the data according to the percentage distribution on the gradient, we found that increased CD36 mRNA was associated with putative polysome fractions from high-glucose-treated cells relative to loading controls (Figures 5G and 5H). These data suggested that glucose stress enhanced CD36 translation at an early stage.

At later time points, mRNA and protein levels of CD36 had increased *in vivo* and *in vitro* (Figures 5C and 5E). These data suggested that while CD36 was upregulated by a translational mechanism at the early stage of the hyperglycemic response, transcriptional mechanisms may also be involved after prolonged hyperglycemic treatment. Therefore, the early induction of CD36 may serve as a triggering factor in the CD36/miR-320 regulatory loop.

Loss of Ago2 mediated the early induction of CD36 by hyperglycemia

Considering the potential translational regulation of CD36 in the early stage of hyperglycemia, we tested whether Ago2, a core RNA-induced silencing complex (RISC) component that usually negatively regulates gene expression at translational levels, was involved in this process. We observed a significant decrease in Ago2 expression in cardiomyocytes after 3 h of high-glucose treatment (Figure 6A). An *in vivo* study also revealed a decrease in cardiac Ago2 levels in early-stage diabetes (Figures 6B and 6C). To identify the cause-and-effect relationship between the Ago2 loss and CD36 induction, Ago2-specific siRNA was used to knock down Ago2 expression. Ago2 knockdown increased CD36 protein levels without affecting its mRNA expression (Figures 6D and 6E). This suggested that hyperglycemia might inhibit Ago2 expression, leading to CD36 mRNA detachment from Ago2/RISC, which in turn activates CD36 translation (Figure 6F). RNA immunoprecipitation (RIP)-Ago2 confirmed this hypothesis by showing the decreased binding of CD36 mRNA to Ago2 in cardiomyocytes treated with high glucose (Figure 6G).

The detailed mechanism underlying the hyperglycemia-induced Ago2 loss in the early stage of diabetes is still unknown. The Ago2 mRNA levels were not affected by hyperglycemia (Figure 6H). In addition, Ago2 translation activity remained invariant in the early stage of high glucose treatment (Figure S7A). We then detected Ago2 secretion into the plasma or cell culture supernatant. Ago2 presence in the cell culture supernatant was increased after 3 h of hyperglycemia treatment and returned to the baseline after 12 h (Figure 6I). Increased secretion of Ago2 into the circulation during diabetes was also observed in diabetic human plasma (Figure 6J, Table S8). Furthermore, we isolated exosomes from human plasma and found that Ago2 was detectable in the exosomes (Figure S8, Table S9). Moreover, considering that Ago2 ubiquitination plays a central role in its turnover,[36] Ago2 degradation was studied by detecting ubiquitin level. We observed an upregulation of the ubiquitinated Ago2 protein with high-glucose treatment (Figure 6K). Furthermore, high-glucose-induced Ago2 downregulation was abolished by pretreatment with MG132, a potent inhibitor of the ubiquitin-protease pathway (Figure 6L).

These data suggested that during the early stage of diabetes, CD36 translational upregulation was likely achieved by the Ago2 reduction, which might be due to the increased secretion to the extracellular space and enhanced degradation by the ubiquitin-protease pathway.

DISCUSSION

The present findings, coupled with our previous study,[27] suggested the existence of a positive feedback loop involving miR-320 and CD36 in the onset and continuing manifestation of the DCMP phenotype (Figure S9). Specifically, our previous study revealed that miR-320 translocated to the nucleus to enhance CD36 transcription, which promotes FAA uptake and myocardial lipid deposition, eventually leading to DCMP. The current study demonstrated a positive regulatory loop between CD36 and miR-320, with CD36 induction

Figure 3. miR-320 knockdown protected against diastolic dysfunction in db/db mice

(A) Time course analysis of random-fed blood glucose levels in wild-type (WT), db/db-control, db/db-rAAV-GFP, db/db-rAAV-miR-320, db/db-rAAV-miR-320-TuD, db/db-insulin groups. N = 8. (B)–(D) Echocardiographic and hemodynamic analysis of wild-type mice and db/db mice in different groups. dp/dt max and dp/dt min, peak instantaneous rate of LV pressure increase and decrease, respectively. N = 7–10. (E) Cardiac lipid deposition detected by oil red staining in different groups. N = 5–6. (F) Cardiomyocytes visualization and size quantitation by H&E staining in different groups. N = 5–6. (A)–(F) $^{**}p < 0.01$, $^{***}p < 0.001$; (A)–(F) one-way ANOVA.

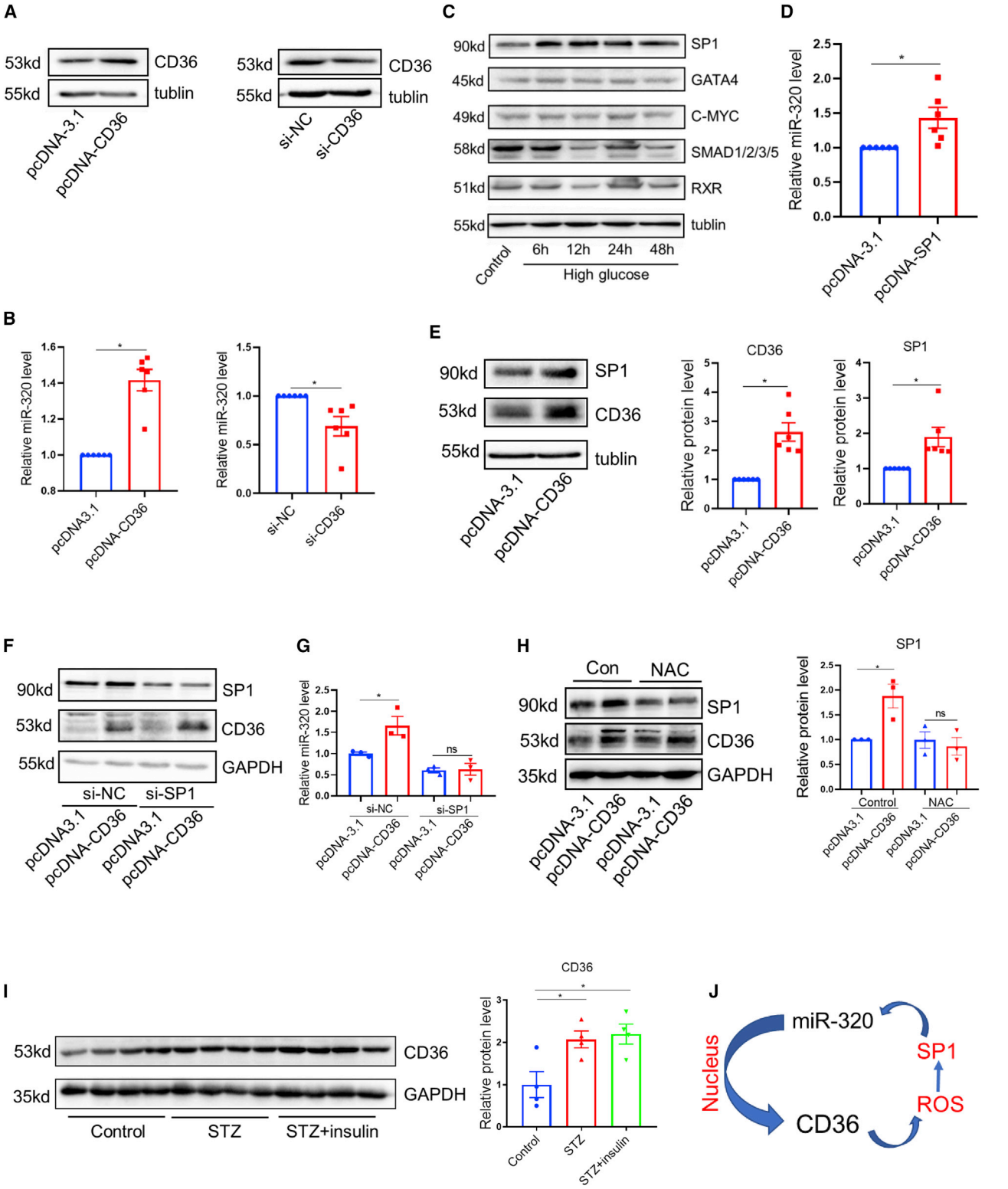

(legend on next page)

as an early trigger that later induced miR-320 expression. In addition, CD36 increase in the early stage of DCMP was likely mediated by the decreased Ago2 protein involved in targeted degradation. Once established, this feedback loop persisted even after the normalization of hyperglycemia in the diabetic model, which may explain the hyperglycemic memory phenomenon in the diabetic heart. Our *in vivo* study showed that rAAV-miR-320 TUD-mediated inhibition of miR320 restored cardiac diastolic function, serving as a potential therapeutic strategy for treating DCMP.

As early as 1990, Roy et al. coined the term "metabolic memory" by demonstrating the poor reversibility of diabetic complications after the normalization of glucose levels. In cultured human endothelial cells, high-glucose-induced fibronectin and collagen IV overexpression remained detectable after replating and multiple cell divisions in the presence of normal glucose concentrations. They concluded that hyperglycemia might be responsible for these events through the induction of self-perpetuating changes in gene expression.[37] Over the ensuing years, their hypothesis has received growing experimental support; multiple cellular mechanisms such as advanced glycation, lipotoxicity, oxidative stress, mitochondrial dysfunction, histone acetylation, and methylation may confer sustained modifications to genes and proteins implicated in diabetic complications.[38–41] Our study provides new insights into the potential mechanisms of hyperglycemic memory, involving a positive feedback loop between miR-320 and the FFA transport gene CD36. CD36 is a scavenger receptor that functions in high-affinity tissue uptake FFAs and contributes to lipid accumulation and metabolic dysfunction under excessive fat supply.[42] Lipotoxicity is a process by which lipid accumulation in non-adipose organs results in oxidative stress, mitochondrial dysfunction, and apoptosis, leading to cellular and tissue dysfunction.[43,44] Sustained CD36 elevation may be responsible for the continued cardiac dysfunction through the induction of self-perpetuating changes in gene expression. miR-320 knockdown inhibited this regulatory loop and effectively rescued the diastolic dysfunction in type 1 and type 2 diabetic mice.

T1DM is characterized mainly by insulin-dependent hyperglycemia, whereas T2DM involves insulin resistance associated with obesity and hyperlipidemia in skeletal muscle and hepatic tissues.[38] STZ treatment is a well-recognized approach to induce T1DM by destroying pancreatic β cells.[45,46] We showed that the CD36 and miR-320 feedback loop contributed to the DCMP progression in T1DM, even after hyperglycemia had normalized. For T2DM, although other mechanisms such as insulin resistance and inflammation are also involved, clinical guidelines strongly recommend glycemic control to reduce the burden of long-term diabetic complications.[47,48] In this study, we showed that insulin failed to do this, whereas miR-320 knockdown effectively rescued diastolic dysfunction in type 2 diabetic mice. However, considering the coexistence of multiple cardiovascular risk factors in T2DM, other mechanisms such as "hyperlipemia memory" and/or "hyperinsulinemia memory" may be involved in the DCMP progression in T2DM and require further studies. Another issue that needs to be addressed is whether the "hyperglycemia memory" is a side effect of insulin treatment. We have performed islet transplantation on STZ-induced T1DM mice and observed progression of cardiac dysfunction (unpublished data), indicating that "hyperglycemia memory" indeed existed. Although a large number of new antidiabetic agents such as sodium-glucose cotransporter-2 inhibitors are effective in reducing cardiac events, insulin was still selected in this study for glycemic control. This is because insulin remains the fundamental treatment for T1DM and T2DM patients, especially in whom oral hypoglycemic agents are ineffective in reducing glucose levels and those with contraindications to non-insulin antidiabetic agents, such as severe diabetic nephropathy and gestational diabetes.[49,50] Therefore, exploring the mechanisms of "hyperglycemia memory" using insulin for glycemic control may have clinical implications for patients with type 1 and type 2 diabetes.

Although frequently referred to in clinical studies,[51–53] "hyperglycemia memory" is not widely used in basic research, due to the following: (1) lack of well-established animal models and (2) unestablished follow-up time after hyperglycemia normalization in animal models. The follow-up times in human studies (usually years or decades) are yet to be extended to animal studies. This is a major challenge in studying "hyperglycemia memory" in animal models for the entire research community. We selected several observed time points (4, 8, and 12 weeks) for our study based on our experience; however, we were unable to rule out the possibility that "hyperglycemia memory" was the delayed structural change in the myocardium. Therefore, further studies are required to establish an appropriate follow-up time for animal studies that is comparable to that of patients with diabetes.

Clinically, heart failure with preserved ejection fraction (HFpEF) has emerged as a significant issue in patients with DM. Despite the lack of consensus on the pathophysiology of the disease, both American and European heart failure guidelines have based the HFpEF diagnostic criteria on clinical parameters, including preserved EF and diastolic

Figure 4. The CD36/miR-320 positive feedback loop in cardiomyocytes

(A) Western blotting analysis of CD36 protein levels in AC-16 cells transfected with pcDNA-CD36 or si-CD36. (B) Quantitative real-time PCR analysis of miR-320 in AC-16 cells transfected with pcDNA-CD36 or si-CD36. N = 6. (C) Western blotting analysis of TFs levels in AC-16 cells treated with high glucose (high glucose: 33.3 mM; control glucose: 5.5 mM). (D) Quantitative real-time PCR analysis of miR-320 in AC-16 cells transfected with pcDNA-SP1. N = 6. (E) Western blotting analysis of SP1 protein levels in AC-16 cells transfected with pcDNA-CD36. N = 3. (F) Western blotting analysis of CD36 and SP1 in AC-16 cells transfected with pcDNA-CD36 under si-NC or si-SP1 conditions. (G) Quantitative real-time PCR analysis of miR-320 in in AC-16 cells transfected with pcDNA-CD36 under si-NC or si-SP1 conditions. N = 3. (H) Western blotting of SP1 protein levels in AC-16 cells transfected with pcDNA-CD36 under NAC (N-acetyl cysteine) or control treatment. N = 3. (I) Western blotting analysis of cardiac CD36 protein levels in diabetic mice 8 weeks after STZ treatment with 4 weeks glycemic control by insulin. N = 4. (J) A model to illustrate the positive feedback loop between CD36 and miR-320. (A)–(J) *$p < 0.05$; (B)–(E) Wilcoxon signed-rank test; (G)–(I) one-way ANOVA.

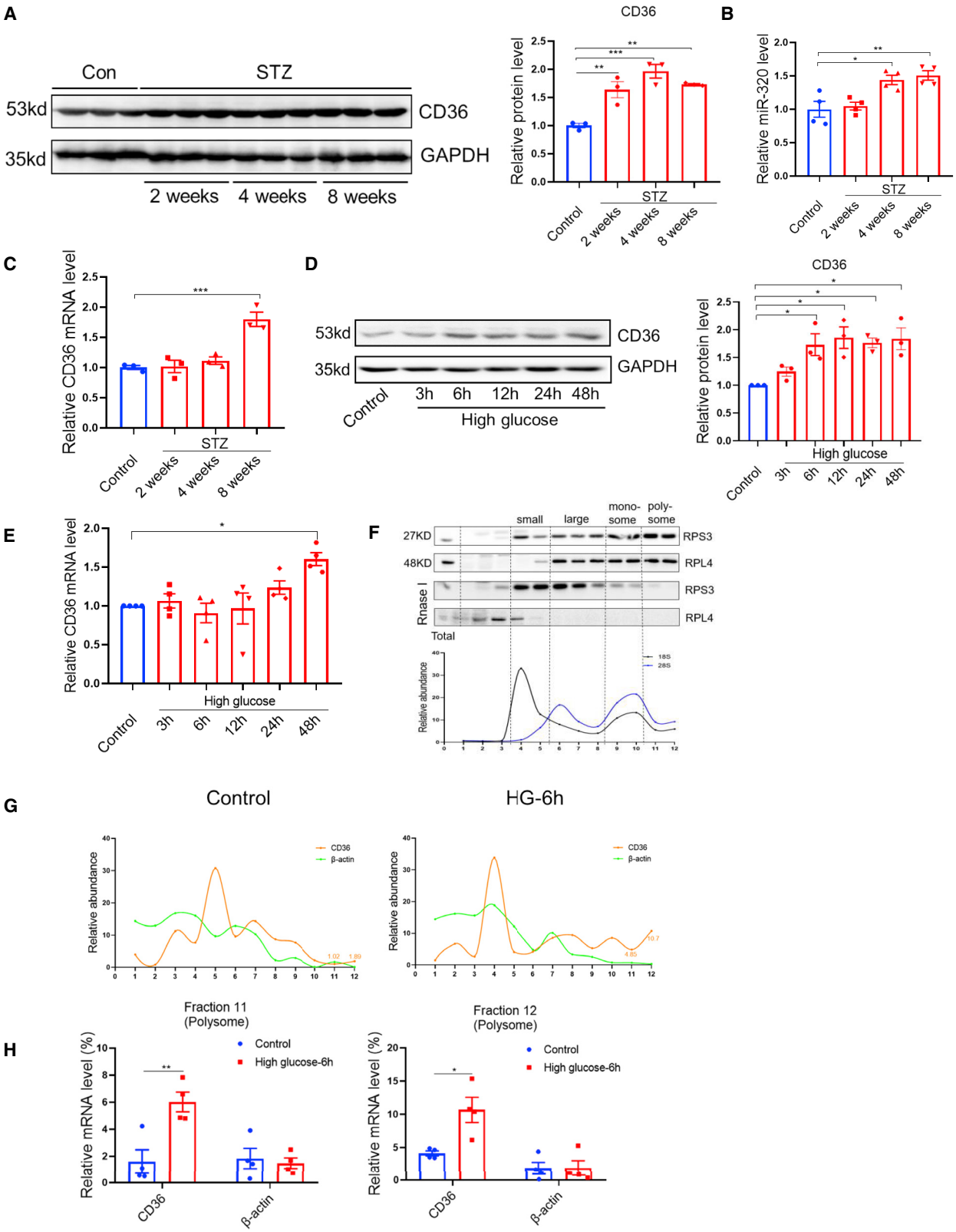

(legend on next page)

parameters evaluated using echocardiography or catheterization.[54] Therefore, we focused on evaluating cardiac diastolic function in DCMP. There are several mechanisms that result in phenotypical HFpEF, including increased myocardial collagen deposition, impaired cardiac metabolism and substrate utilization, myocardial steatosis (lipid accumulation), altered insulin signaling-induced protein kinase C activation, advanced glycated end-product deposition, and impaired endothelial nitric oxide production.[22,55] In our study, we did not observe any changes in myocardial fibrosis following miR-320 knockdown. We observed increased cardiac lipid accumulation in the heart of diabetic mice, which was alleviated by miR-320 knockdown, suggesting that the miR-320-CD36 loop may influence diastolic dysfunction of DCMP by promoting cardiac lipid accumulation.

The well-studied miR-320 has been implicated in multiple metabolic and cardiovascular diseases. As early as 2009, miR-320 expression was found to be decreased in hearts with ischemia/reperfusion; transgenic mice with cardiac-specific miR-320 overexpression showed increased apoptosis and infarction size, while miR-320 knockdown reduced the infarction size.[56] Another study demonstrated that miR-320a induces diabetic nephropathy via inhibiting MafB,[57] mediates doxorubicin-induced cardiotoxicity by targeting the vascular endothelial growth factor signaling pathway, and contributes to atherogenesis by augmenting multiple risk factors and downregulating serum response factor (SRF).[24,58] In DCMP, miR-320 upregulation in the heart of high-fat diet-, db/db-, and STZ-treated mice acts in the nucleus to enhance CD36 transcription, contributing to cardiac dysfunction.[27] Furthermore, this study demonstrated that glycemic control does not restore hyperglycemia-induced alterations in miR-320 expression, indicating a potential miR-320 role in hyperglycemic memory. In contrast with insulin treatment, miR-320 knockdown protected against the onset of diastolic dysfunction in the STZ-treated mice. We observed only mild miR-320 upregulation (between 1.5- and 2-fold) in the heart of STZ-treated mice. Considering that cardiac cells are a mixture of multiple cell types, we isolated CMs and non-CMs, and we found that miR-320 upregulation was specifically detected in CMs; but a trend of decreased miR-320 expression was observed in non-CMs in the STZ-treated mouse hearts. A previous study showed that in mice with transverse aortic constriction (TAC)-induced heart failure, miR-320 overexpression in CMs exacerbated cardiac dysfunction, whereas miR-320 overexpression in cardiac fibroblasts (CF) alleviated cardiac fibrosis and hypertrophy.[59] In diabetic hearts, it is possible that CF-localized miR-320 may be protective against cardiac performance. However, CF-localized miR-320 did not seem to participate in the CD36/miR-320 loop because miR-320 was localized in the cytoplasm[27] and was therefore unable to induce CD36 transcription.

We found that miR-320 TUD-mediated inhibition rescued diastolic dysfunction, and miR-320 mimic expression did not further exacerbate diastolic dysfunction in the diabetic mouse heart. This was possibly due to the following: (1) miR-320 expression may require more time to exhibit its effect; (2) miR-320 is necessary but not sufficient for the formation of the feedback loop. Moreover, despite clear upregulation of a single myocytes area in diabetic mice, we did not detect significant morphological changes in whole heart sections between various groups (Figures S3E and S4C). This was possibly because the wall thickness of the whole heart section was determined by (1) the area of single myocytes and (2) the number of myocytes. In fact, myocyte apoptosis was dramatically increased in diabetic hearts.[27] Therefore, an increase in the area of a single myocyte may not affect the overall hypertrophy in the whole heart section because of the decrease in myocytes numbers.

In the positive feedback loop, we concluded that CD36 was the initiation factor because increased CD36 protein expression in early DM was consistent with enhanced CD36 translation as detected by polysome analysis, but it was not coupled with increased mRNA levels. We observed a decreased Ago2 level in the early hyperglycemia stages both *in vivo* and *in vitro*, which seemed to directly regulate CD36 protein translation based on targeted knockdown results. Ago2-mediated CD36 translational regulation might be contributed by other unknown miRNAs. At later stages of diabetes, Ago2 protein levels returned to normal, and CD36 protein and mRNA levels were upregulated, possibly resulting from miR-320-mediated transcriptional activation.

In this study, we found that Ago2 was secreted outside of cells in diabetes. Previous studies have also detected Ago2 in cell culture media and human blood plasma.[60,61] Moreover, Ago2 translocates into exosomes, a critical process for Ago2-bound miRNAs, such as let-7a, miR-100, and miR-320a, to transport into extracellular exosomes from cancer cells.[62,63] In cardiovascular diseases, composition changes in exosomes under pathological conditions contribute to disease development. Exosomes did not affect cardiac function in any unifying

Figure 5. CD36 was the initial factor of CD36/miR-320 positive feedback loop at the early stage of hyperglycemia

(A) Time course analysis of CD36 protein levels in diabetic mice 2, 4, and 8 weeks after STZ treatment. N = 3. (B) Time course analysis of relative miR-320 levels in diabetic mice 2, 4, and 8 weeks after STZ treatment. N = 4. (C) Time course analysis of relative CD36 mRNA levels in diabetic mice 2, 4, and 8 weeks after STZ treatment. N = 3. (D) Time course analysis of CD36 protein levels in AC-16 cells after 3, 6, 12, 24, and 48 h of high glucose. N = 3. (E) Time course analysis of relative CD36 mRNA levels in AC-16 cells after 3, 6, 12, 24, and 48 h of high glucose. N = 4. (F) Polysome profiling. Representative ribosomal proteins (RPS3 and RPL4) on individual gradient fractions were detected by western blotting, and specific rRNA, mRNA transcripts were quantified by quantitative real-time PCR. The assignment of small and large ribosomal subunits, monosomes, and putative polysomes was based on the distribution of both rRNAs and protein. The putative polysome fractions were characterized by RNase I treatment. The relative abundance of individual transcripts in each fraction was presented as the percentage of the total fraction. (G)–(H) The association of the CD36 mRNA with putative polysome fractions (fraction 11 and 12) in response to 6 h of high glucose treatment (HG-6h). N = 4. (A)–(H) *$p < 0.05$, **$p < 0.01$, ***$p < 0.001$; (A)–(E) one-way ANOVA; (H) Student's t test. High glucose: 33.3 mM; control glucose: 5.5 mM.

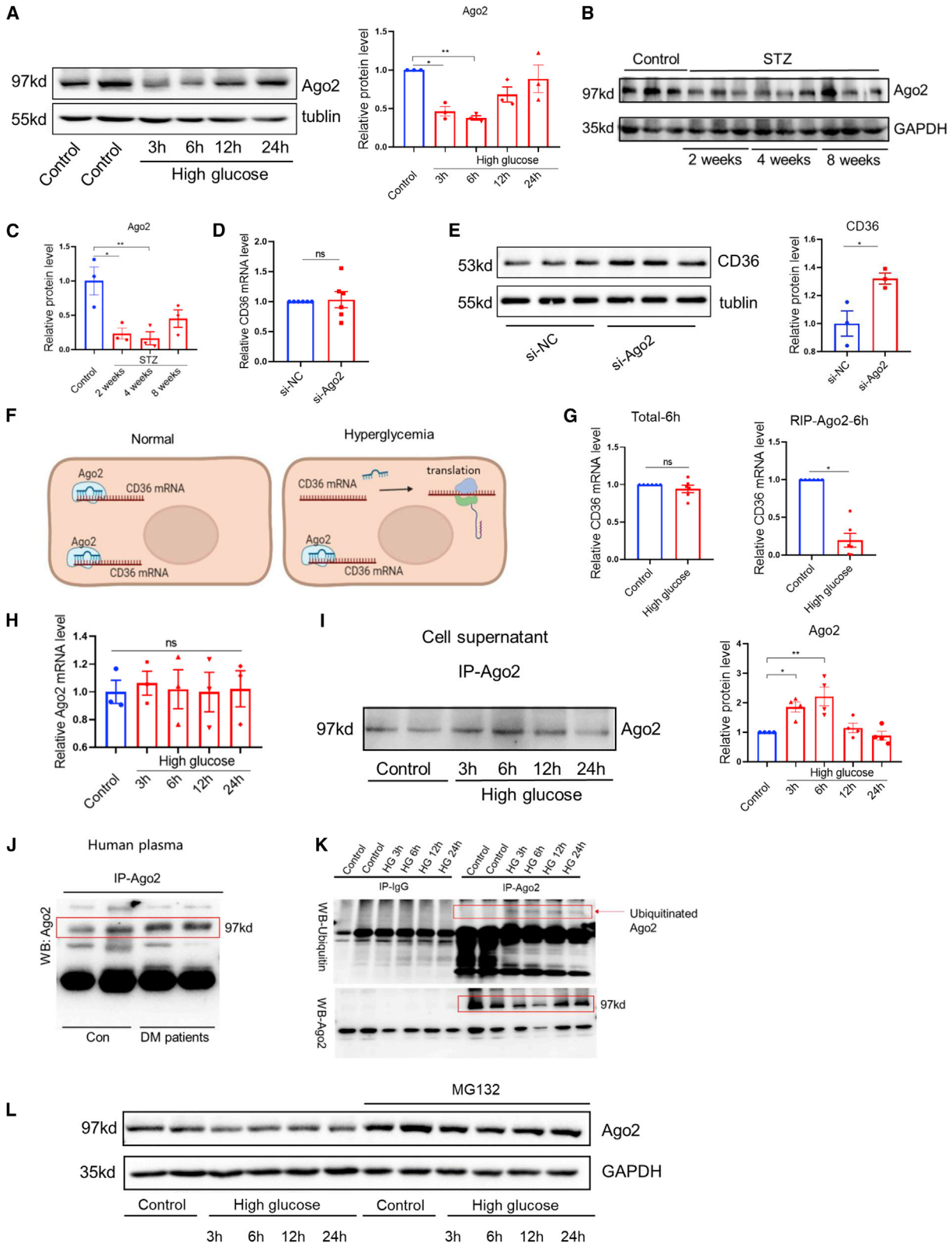

(legend on next page)

direction, and their functions were largely dependent on the contained miRNAs or proteins. Some exosome components were cardio-protective (such as miR-21-5p), while others were detrimental (such as miR-21-3p and miR-320) for cardiac function.[64–66] However, the role of exosomal Ago2 in cardiovascular diseases has not been elucidated. It is possible that exosomal Ago2 secreted from myocytes together with specific Ago2-bound miRNA collectively regulate the function of other cardiac cells (cardiac fibroblasts and cardiac endothelial cells) or other tissues during diabetes-induced complications. Further studies are needed to reveal the complicated crosstalk between different cells or tissues mediated by exosomal Ago2 and bound miRNAs. Apart from secretion into the cell culture supernatant by high glucose, Ago2 degradation through the ubiquitin-proteasome pathway also increased. The correlation between increased Ago2 secretion and degradation also requires further study.

In summary, our findings reveal that in DCMP, miR-320 and CD36 mutually enhance the expression of one another, leading to a positive feedback loop and possible hyperglycemic memory in cardiomyocytes. We demonstrated that miR-320 inhibition could rescue diastolic dysfunction in diabetic mice. These findings provide proof-of-concept evidence of a potential therapeutic strategy for the treatment of DM-induced cardiac dysfunction by targeting miR-320.

MATERIALS AND METHODS

Ethics

All animal studies were conducted with the approval of the Animal Research Committee of Tongji Medical College and in accordance with the NIH Guide for the Care and Use of Laboratory Animals (ethics permit number: TJH-201904010). To avoid the potential effects of sex differences, male C57BL/6J mice, db/db mice on C57BL/Ks background, and control C57BL/Ks mice (GemPharmatech, Nanjing, China) were used. Because of the possible effects of estrogens on the heart, only adult male mice were used for all experiments. Mice were anesthetized with intraperitoneal injections of a mixture of xylazine (5 mg/kg) and ketamine (80 mg/kg), and all efforts were made to minimize suffering.

Human plasma

Human plasma was studied according to a protocol approved by the Clinical Research Committee of Tongji Medical College (ethics permit number: NCT03461107). The study conformed to the principles outlined in the Declaration of Helsinki (2000). Five patients with diabetes and five controls were recruited in the study and provided informed consent. Patients with diabetes were selected based on a fasting plasma glucose concentration of $\geq$7.0 mmol/L.

STZ treatment

STZ (Sigma-Aldrich, Shanghai, China) was dissolved in sodium citrate buffer (pH = 4.5) to a concentration of 8 mg/mL. C57BL/6J mice (8-week-old males) were deprived of food overnight and then injected intraperitoneally with 40 mg/kg STZ for 5 consecutive days. The control mice were injected with an equivalent volume of sodium citrate buffer as previously suggested.[3] Blood glucose levels in the tail veil of all experimental mice were measured using a blood glucometer (OneTouch Verio Vue, OneTouch, Shanghai, China); a range of $\geq$13.3 mmol/L was considered diabetic. The mice were sacrificed via cervical dislocation. The detailed experimental procedures are presented in Figure S1.

Insulin pump implantation and subcutaneous insulin injection

The STZ-induced diabetic mice in the blood glycemic control group were anesthetized with 1% pentobarbital and implanted with an Alzet Mini-Osmotic Pump 1004 (Durect, Cupertino, CA),[3] which was supplemented with insulin aspart injection (NovoRapid FlexPen, Novo Nordisk, Bagsvaerd, Denmark). Db/db mice in the blood glycemic control group were subcutaneously injected with 2 U/kg of insulin glargine once a day.[67] Detailed information on the animal studies is shown in the Figure S1.

rAAV administration

rAAVs (type 9) containing miR-320, miR-320 TUD, or GFP were prepared by triple plasmid co-transfection in HEK293T cells as previously described.[22] The rAAV-D(+) vector (double-stranded rAAV vector plasma), adenovirus helper plasmid phelper, and packaging plasmid pXX9 were kindly provided by Dr. Xiao.[68,69] For the *in vivo* experiments, control or STZ-treated mice were randomly divided into different groups: NS (1X PBS), rAAV-GFP, rAAV-miR-320, rAAV-miR-320 TUD. Db/db mice and their litter controls were also divided into several groups, including the four mentioned. rAAV viruses carrying 1×10^{11} vector copies dissolved in 100 μL of 1 × PBS were administrated by a one-time tail vein injection into the STZ or db/db mouse model. The detailed numbers for each group are presented in the figure legends (Figure S1 legend).

Figure 6. Loss of Ago2 mediated the early induction of CD36 by hyperglycemia

(A) Time course analysis of Ago2 protein levels in AC-16 cells after 3, 6, 12, 24, and 48 h of high glucose. N = 3. (B) Time course analysis of Ago2 protein levels from heart in diabetic mice 2, 4, and 8 weeks after STZ treatment. (C) Quantitative analysis of Ago2 protein levels in diabetic mice. N = 3. (D) Quantitative real-time PCR analysis of CD36 mRNA levels in AC-16 cells transfected with si-Ago2. N = 6. (E) Western blotting analysis of CD36 in AC-16 cells transfected with si-Ago2. N = 3. (F) A model illustrating how Ago2 reduction stimulated CD36 translation. (G) Left: quantitative real-time PCR analysis of total CD36 mRNA level in AC-16 cells after 6 h of hyperglycemia. N = 6; Right: quantitative real-time PCR analysis of CD36 mRNA immunoprecipitated from AC-16 cells with anti-Ago2 after 6 h of hyperglycemia. N = 6. (H) Time course analysis of relative Ago2 mRNA levels in AC-16 cells after 3, 6, 12, and 24 h of high glucose. N = 3. (I) Immunoprecipitation of Ago2 protein from cell culture supernatant with anti-Ago2 after 3, 6, 12, and 24 h of hyperglycemia on AC-16 cells. N = 3. (J) Immunoprecipitation of Ago2 protein with anti-Ago2 antibody from plasma of diabetic patients. (K) Ubiquitinated Ago2 levels in AC-16 cells after 3, 6, 12, and 24 h of high glucose (HG). (L) Western blotting analysis of Ago2 in AC-16 cells treated with MG132 after 3, 6, 12, and 24 h of high glucose. (A)–(L) RIP: RNA immunoprecipitation. High glucose: 33.3 mM. Control glucose: 5.5 mM. *$p < 0.05$, **$p < 0.01$; (A), (C), (H), and (I) one-way ANOVA; (D) and (G) Wilcoxon signed-rank test; (E) Student's t test.

Cell culture and transfection

HEK293 and AC 16 cells from ATCC (Manassas, VA, Designation No. PTA-1500) were maintained in H-DMEM supplemented with 10% FBS at 37°C in a 95% air and 5% CO_2 atmosphere. AC16 cells were incubated with normal (5 mM) or high (33 mM) glucose for 3 h, 6 h, 12 h, 24 h, and 48 h and then collected. miRNA mimics, siRNAs, and relative controls were purchased from RiboBio (Guangzhou, China), the catalog numbers are listed in Table S10. Transfection with miR-320 mimics (100 nM), siRNAs (100 nM), and relative controls (100 nM) was performed using Lipofectamine 2000 (Invitrogen, Carlsbad, CA), according to the manufacturer's recommendations. Specifically, serum-free complexes using a DNA (μg) to Lipofectamine 2000 (μL) ratio of 1:3 were prepared for plasmid DNA transfection; for miRNA or siRNA, complexes containing 100 pmol RNA and 3μL Lipofectamine 2000 were prepared. The medium was changed 6 h after transfection.

RNA extraction and quantitative real-time PCR

Total RNA was extracted from cells or frozen tissues using TRIzol followed by reverse transcription with the SuperScript III First Strand Synthesis Kit (Life Technologies, Carlsbad, CA, USA). Real-time PCR assays were performed according to the manufacturer's instructions using the SYBR Select Master Mix (Life Technologies, Carlsbad, CA) on a 7900HT FAST Real-Time PCR System (Life Technologies, Carlsbad, CA).[26] All reactions were performed in triplicates.

Polysome analysis

Sucrose gradient sedimentation of the ribosome/polysome was performed as previously described.[26,70] Briefly, AC-16 cells were treated with cycloheximide (100 μg/mL) and suspended in a lysis buffer on ice for 30 min. The lysate (400 μL each) was then loaded onto a 10%–50% sucrose gradient and centrifuged at 180,000 g for 260 min in an SW40.1 Ti Rotor (Beckman Coulter, Fullerton, CA, USA). After centrifugation, 12 gradient fractions were collected for RNA and protein analyses. Representative ribosomal proteins (RPS3 and RPL4) were measured using western blotting, and specific RNAs were quantified using quantitative real-time PCR. The assignment of small and large ribosomal subunits, monosomes, and putative polysomes was based on the distribution of rRNAs and ribosomal proteins. To characterize the putative polysomes, the lysate was treated with 5 U/ml RNase I for 40 min at 25°C to convert polysomes to monosomes. The relative abundance of individual transcripts in each fraction was presented as a percentage of the total fraction.

RNA immunoprecipitation

The cell lysis solution was immunoprecipitated with anti-Ago2 antibody (Abnova Corporation, Taiwan, China) or IgG (Santa Cruz Biotechnology, Santa Cruz, CA) using protein G Sepharose beads (Santa Cruz Biotechnology, Santa Cruz, CA). After elution from the beads, bound RNA was extracted with TRIzol and quantified by real time RT-PCR.

Protein extraction and western blotting

Protein samples from cells or frozen hearts were quantified by using bicinchoninic acid assay kit (BOSTER, Wuhan, China). For western blotting, total cell lysate was re-dissolved by SDS-PAGE, transferred to nitrocellulose membrane, and blocked with 5% non-fat dry milk in TBS-T. The membrane was incubated with indicated primary antibody overnight at 4°C, followed by incubation with peroxidase-conjugated secondary antibody for 2 h, and finally developed using the ECL system (Beyotime Institute of Biotechnology, Nanjing, China). The antibodies used in this study are listed in Table S11. Western blotting results were quantified by densitometry and processed with the ImageJ software (National Institutes of Health software, USA).

Transcription factor prediction

To predict TFs that bind to the promotor region of miR-320, TRANSFAC 2.0 (http://www.gene-regulation.com/index2.html) and JASPAR (https://jaspar.genereg.net/) databases were employed. The 5′ promoter region (approximately 0–2000 bps) of DNA was selected for prediction.

Cardiac echocardiography

After anesthetization, echocardiography was performed with a 30-MHz 30 high-frequency scan head (VisualSonics Vevo1100, VisualSonics, Toronto, ON, Canada) as we described previously.[22,23,71] Briefly, a parasternal long-axis B-mode image was acquired with appropriate positioning of the scan head so that the maximum LV length could be identified. Then a clockwise 90° rotation at the papillary muscle level depicted the parasternal short-axis view. From this view, an M-mode cursor was positioned perpendicular to the anterior and posterior walls of the left ventricle, and M-mode image loops were obtained for measurement of wall thickness and chamber dimensions. LVEF was calculated as follows: LVEF = (left ventricular end-diastolic volume [LVEDV] – left ventricular end-systolic volume [LVESV])/LVEDV ×100%. FS was calculated as follows: FS% = (left ventricular end diastolic dimension [LVDd] –left ventricular end systolic dimensions [LVDs])/LVDd × 100%. For evaluation of diastolic function of left ventricle, pulse wave Doppler imaging and tissue Doppler imaging were used as previous described.[72,73] Specifically, the scan head was positioned in an apical four-chamber view. Transmitral inflow was obtained in pulse wave Doppler mode, for measuring the peak velocity of early (E peak) and late (A peak) filling of mitral inflow. The tissue motion velocity of mitral annulus was measured in tissue Doppler mode, which included a waveform in early diastole (E′ peak). The ratios of E peak to A peak (E/A) as well as E peak to E′ peak (E/E′) were then calculated. Each of these captured image loops included 11 to 20 cardiac cycles, and data were averages from at least three cycles per loop. To monitor left ventricular catheterization, a catheter manometer (Millar 1.4F, SPR 835, Millar Instruments) was inserted via the right carotid artery into the left ventricle. The data were continuously recorded. The cardiac function parameters were calculated with PVAN software (Millar 2 Instruments, Houston, TX), as described.[22]

Histopathology

Formalin-fixed tissues were paraffin embedded and in paraffin, cut into 4-μm-thick sections and stained with hematoxylin and eosin (H&E) and Sirius red. Fresh tissues embedded with cryo-embedding media (OCT) were frozen completely, sectioned into 10-μm thickness

using a cryotome and stained with oil red. Images were acquired using a light microscope. Six areas were randomly selected from each section and automatically quantified using the Image-Pro Plus software (version 6.0; Media Cybernetics, Bethesda, MD, USA).

Statistical analysis

Data are presented as mean ± SEM (n is noted in specific figure legends). All datasets were tested for normality typically using the Shapiro-Wilk test to choose an appropriate parametric or nonparametric test. Student's t tests were performed to determine statistical significance between two groups. One-way ANOVA combined with Tukey's multiple comparisons were performed for comparisons among more than two groups. Wilcoxon signed-rank tests were applied for nonparametric paired analysis (two groups). In all cases, statistical significance was defined as $p < 0.05$.

DATA AVAILABILITY STATEMENT

The authors declare that all data supporting the findings of this study are available within the paper and its supplemental information files.

SUPPLEMENTAL INFORMATION

Supplemental information can be found online at https://doi.org/10.1016/j.omtn.2022.12.009.

ACKNOWLEDGMENTS

We thank our colleagues in Dr. Wang's group for technical assistance and stimulating discussions during the course of this investigation. This work was supported by grants from the National Natural Science Foundation of China (nos. 82170273, 81822002, 31800973, 31771264, 91839302, 81630010, and 81790624) and Wuhan Aurora Project 2022020801020451. The funders had no role in study design, data collection and analysis, manuscript preparation, or decision to publish.

AUTHOR CONTRIBUTIONS

J.Z. and K.J. designed the study, analyzed and interpreted the data, and drafted the paper; N.D., Y.Z., G.H., S.Y., R.X., and Z.W., participated in acquiring the data; and C.C., H.L., and D.W.W. designed the work and drafted the paper.

DECLARATION OF INTERESTS

The authors declare no competing interests.

REFERENCES

1. Saeedi, P., Petersohn, I., Salpea, P., Malanda, B., Karuranga, S., Unwin, N., Colagiuri, S., Guariguata, L., Motala, A.A., Ogurtsova, K., et al. (2019). Global and regional diabetes prevalence estimates for 2019 and projections for 2030 and 2045: results from the international diabetes federation diabetes atlas. Diabetes Res. Clin. Pract. *157*, 107843. 9(th) edition.
2. Haffner, S.M., Lehto, S., Rönnemaa, T., Pyörälä, K., and Laakso, M. (1998). Mortality from coronary heart disease in subjects with type 2 diabetes and in nondiabetic subjects with and without prior myocardial infarction. N. Engl. J. Med. *339*, 229–234.
3. Costantino, S., Paneni, F., Lüscher, T.F., and Cosentino, F. (2016). MicroRNA profiling unveils hyperglycaemic memory in the diabetic heart. Eur. Heart J. *37*, 572–576.
4. Guo, R., and Nair, S. (2017). Role of microRNA in diabetic cardiomyopathy: from mechanism to intervention. Biochim. Biophys. Acta, Mol. Basis Dis. *1863*, 2070–2077.
5. Huynh, K., Bernardo, B.C., McMullen, J.R., and Ritchie, R.H. (2014). Diabetic cardiomyopathy: mechanisms and new treatment strategies targeting antioxidant signaling pathways. Pharmacol. Ther. *142*, 375–415.
6. Vinayagan, A., Verma, G.C., and Wahid, A. (2020). The prevalence of diastolic dysfunction in diabetic mellitus in the age group of 20-40 Years and its correlation with duration of diabetes, HBA1C level and diabetic retinopathy. J. Assoc. Physicians India *68*, 51.
7. von Bibra, H., and St John Sutton, M. (2010). Diastolic dysfunction in diabetes and the metabolic syndrome: promising potential for diagnosis and prognosis. Diabetologia *53*, 1033–1045.
8. Tan, Y., Zhang, Z., Zheng, C., Wintergerst, K.A., Keller, B.B., and Cai, L. (2020). Mechanisms of diabetic cardiomyopathy and potential therapeutic strategies: preclinical and clinical evidence. Nat. Rev. Cardiol. *17*, 585–607.
9. Jia, G., Hill, M.A., and Sowers, J.R. (2018). Diabetic cardiomyopathy: an update of mechanisms contributing to this clinical entity. Circ. Res. *122*, 624–638.
10. Gilbert, R.E., and Krum, H. (2015). Heart failure in diabetes: effects of anti-hyperglycaemic drug therapy. Lancet *385*, 2107–2117.
11. Ceriello, A. (2009). Hypothesis: the "metabolic memory", the new challenge of diabetes. Diabetes Res. Clin. Pract. *86*, S2–S6.
12. Prattichizzo, F., Giuliani, A., De Nigris, V., Pujadas, G., Ceka, A., La Sala, L., Genovese, S., Testa, R., Procopio, A.D., Olivieri, F., and Ceriello, A. (2016). Extracellular microRNAs and endothelial hyperglycaemic memory: a therapeutic opportunity? Diabetes Obes. Metab. *18*, 855–867.
13. Felekkis, K., Touvana, E., Stefanou, C., and Deltas, C. (2010). microRNAs: a newly described class of encoded molecules that play a role in health and disease. Hippokratia *14*, 236–240.
14. Lu, T.X., and Rothenberg, M.E. (2018). MicroRNA. J. Allergy Clin. Immunol. *141*, 1202–1207.
15. Schanen, B.C., and Li, X. (2011). Transcriptional regulation of mammalian miRNA genes. Genomics *97*, 1–6.
16. Zhou, Q., Lv, D., Chen, P., Xu, T., Fu, S., Li, J., and Bei, Y. (2014). MicroRNAs in diabetic cardiomyopathy and clinical perspectives. Front. Genet. *5*, 185.
17. Melman, Y.F., Shah, R., and Das, S. (2014). MicroRNAs in heart failure: is the picture becoming less miRky? Circ. Heart Fail. *7*, 203–214.
18. Das, S., Ferlito, M., Kent, O.A., Fox-Talbot, K., Wang, R., Liu, D., Raghavachari, N., Yang, Y., Wheelan, S.J., Murphy, E., and Steenbergen, C. (2012). Nuclear miRNA regulates the mitochondrial genome in the heart. Circ. Res. *110*, 1596–1603.
19. Harada, M., Luo, X., Murohara, T., Yang, B., Dobrev, D., and Nattel, S. (2014). MicroRNA regulation and cardiac calcium signaling: role in cardiac disease and therapeutic potential. Circ. Res. *114*, 689–705.
20. Fan, J., Li, H., Nie, X., Yin, Z., Zhao, Y., Zhang, X., Yuan, S., Li, Y., Chen, C., and Wang, D.W. (2018). MiR-665 aggravates heart failure via suppressing CD34-mediated coronary microvessel angiogenesis. Aging *10*, 2459–2479.
21. Nie, X., Fan, J., Li, H., Yin, Z., Zhao, Y., Dai, B., Dong, N., Chen, C., and Wang, D.W. (2018). miR-217 promotes cardiac hypertrophy and dysfunction by targeting PTEN. Mol. Ther. Nucleic Acids *12*, 254–266.
22. Dai, B., Li, H., Fan, J., Zhao, Y., Yin, Z., Nie, X., Wang, D.W., and Chen, C. (2018). MiR-21 protected against diabetic cardiomyopathy induced diastolic dysfunction by targeting gelsolin. Cardiovasc. Diabetol. *17*, 123.
23. Chen, C., Yang, S., Li, H., Yin, Z., Fan, J., Zhao, Y., Gong, W., Yan, M., and Wang, D.W. (2017). Mir30c is involved in diabetic cardiomyopathy through regulation of cardiac autophagy via BECN1. Mol. Ther. Nucleic Acids *7*, 127–139.
24. Chen, C., Wang, Y., Yang, S., Li, H., Zhao, G., Wang, F., Yang, L., and Wang, D.W. (2015). MiR-320a contributes to atherogenesis by augmenting multiple risk factors and down-regulating SRF. J. Cell Mol. Med. *19*, 970–985.
25. Yin, Z., Zhao, Y., Li, H., Yan, M., Zhou, L., Chen, C., and Wang, D.W. (2016). miR-320a mediates doxorubicin-induced cardiotoxicity by targeting VEGF signal pathway. Aging *8*, 192–207.

26. Li, H., Zhang, X., Wang, F., Zhou, L., Yin, Z., Fan, J., Nie, X., Wang, P., Fu, X.D., Chen, C., and Wang, D.W. (2016). MicroRNA-21 lowers blood pressure in spontaneous hypertensive rats by upregulating mitochondrial translation. Circulation *134*, 734–751.

27. Li, H., Fan, J., Zhao, Y., Zhang, X., Dai, B., Zhan, J., Yin, Z., Nie, X., Fu, X.D., Chen, C., and Wang, D.W. (2019). Nuclear miR-320 mediates diabetes-induced cardiac dysfunction by activating transcription of fatty acid metabolic genes to cause lipotoxicity in the heart. Circ. Res. *125*, 1106–1120.

28. Baseler, W.A., Thapa, D., Jagannathan, R., Dabkowski, E.R., Croston, T.L., and Hollander, J.M. (2012). miR-141 as a regulator of the mitochondrial phosphate carrier (Slc25a3) in the type 1 diabetic heart. Am. J. Physiol. Cell Physiol. *303*, C1244–C1251.

29. Rawal, S., Nagesh, P.T., Coffey, S., Van Hout, I., Galvin, I.F., Bunton, R.W., Davis, P., Williams, M.J.A., and Katare, R. (2019). Early dysregulation of cardiac-specific microRNA-208a is linked to maladaptive cardiac remodelling in diabetic myocardium. Cardiovasc. Diabetol. *18*, 13.

30. Rawal, S., Munasinghe, P.E., Nagesh, P.T., Lew, J.K.S., Jones, G.T., Williams, M.J.A., Davis, P., Bunton, D., Galvin, I.F., Manning, P., et al. (2017). Down-regulation of miR-15a/b accelerates fibrotic remodelling in the Type 2 diabetic human and mouse heart. Clin. Sci. *131*, 847–863.

31. Jeyabal, P., Thandavarayan, R.A., Joladarashi, D., Suresh Babu, S., Krishnamurthy, S., Bhimaraj, A., Youker, K.A., Kishore, R., and Krishnamurthy, P. (2016). MicroRNA-9 inhibits hyperglycemia-induced pyroptosis in human ventricular cardiomyocytes by targeting ELAVL1. Biochem. Biophys. Res. Commun. *471*, 423–429.

32. Li, H., Dai, B., Fan, J., Chen, C., Nie, X., Yin, Z., Zhao, Y., Zhang, X., and Wang, D.W. (2019). The different roles of miRNA-92a-2-5p and let-7b-5p in mitochondrial translation in db/db mice. Mol. Ther. Nucleic Acids *17*, 424–435.

33. Castro-Mondragon, J.A., Riudavets-Puig, R., Rauluseviciute, I., Lemma, R.B., Turchi, L., Blanc-Mathieu, R., Lucas, J., Boddie, P., Khan, A., Manosalva Pérez, N., et al. (2022). Jaspar 2022: the 9th release of the open-access database of transcription factor binding profiles. Nucleic Acids Res. *50*, D165–D173.

34. Seimon, T.A., Nadolski, M.J., Liao, X., Magallon, J., Nguyen, M., Feric, N.T., Koschinsky, M.L., Harkewicz, R., Witztum, J.L., Tsimikas, S., et al. (2010). Atherogenic lipids and lipoproteins trigger CD36-TLR2-dependent apoptosis in macrophages undergoing endoplasmic reticulum stress. Cell Metab. *12*, 467–482.

35. Lee, H.B., Yu, M.R., Yang, Y., Jiang, Z., and Ha, H. (2003). Reactive oxygen species-regulated signaling pathways in diabetic nephropathy. J. Am. Soc. Nephrol. *14*, S241–S245.

36. Rybak, A., Fuchs, H., Hadian, K., Smirnova, L., Wulczyn, E.A., Michel, G., Nitsch, R., Krappmann, D., and Wulczyn, F.G. (2009). The let-7 target gene mouse lin-41 is a stem cell specific E3 ubiquitin ligase for the miRNA pathway protein Ago2. Nat. Cell Biol. *11*, 1411–1420.

37. Roy, S., Sala, R., Cagliero, E., and Lorenzi, M. (1990). Overexpression of fibronectin induced by diabetes or high glucose: phenomenon with a memory. Proc. Natl. Acad. Sci. USA *87*, 404–408.

38. Bianchi, C., Miccoli, R., and Del Prato, S. (2013). Hyperglycemia and vascular metabolic memory: truth or fiction? Curr. Diab. Rep. *13*, 403–410.

39. Stitt, A.W. (2003). The role of advanced glycation in the pathogenesis of diabetic retinopathy. Exp. Mol. Pathol. *75*, 95–108.

40. Siebel, A.L., Fernandez, A.Z., and El-Osta, A. (2010). Glycemic memory associated epigenetic changes. Biochem. Pharmacol. *80*, 1853–1859.

41. Cooper, M.E., and El-Osta, A. (2010). Epigenetics: mechanisms and implications for diabetic complications. Circ. Res. *107*, 1403–1413.

42. Pepino, M.Y., Kuda, O., Samovski, D., and Abumrad, N.A. (2014). Structure-function of CD36 and importance of fatty acid signal transduction in fat metabolism. Annu. Rev. Nutr. *34*, 281–303.

43. Virtue, S., and Vidal-Puig, A. (2010). Adipose tissue expandability, lipotoxicity and the Metabolic Syndrome–an allostatic perspective. Biochim. Biophys. Acta *1801*, 338–349.

44. Leggat, J., Bidault, G., and Vidal-Puig, A. (2021). Lipotoxicity: a driver of heart failure with preserved ejection fraction? Clin. Sci. *135*, 2265–2283.

45. Riehle, C., and Bauersachs, J. (2018). Of mice and men: models and mechanisms of diabetic cardiomyopathy. Basic Res. Cardiol. *114*, 2.

46. Wu, J., and Yan, L.J. (2015). Streptozotocin-induced type 1 diabetes in rodents as a model for studying mitochondrial mechanisms of diabetic beta cell glucotoxicity. Diabetes Metab. Syndr. Obes. *8*, 181–188.

47. Kahn, S.E., Cooper, M.E., and Del Prato, S. (2014). Pathophysiology and treatment of type 2 diabetes: perspectives on the past, present, and future. Lancet *383*, 1068–1083.

48. Inzucchi, S.E., Bergenstal, R.M., Buse, J.B., Diamant, M., Ferrannini, E., Nauck, M., Peters, A.L., Tsapas, A., Wender, R., and Matthews, D.R. (2015). Management of hyperglycaemia in type 2 diabetes, 2015: a patient-centred approach. Update to a position statement of the American Diabetes Association and the European Association for the Study of Diabetes. Diabetologia *58*, 429–442.

49. American Diabetes Association Professional Practice Committee, Draznin, B., Aroda, V.R., Bakris, G., Benson, G., Brown, F.M., Freeman, R., Green, J., Huang, E., Isaacs, D., et al. (2022). 9. Pharmacologic approaches to glycemic treatment: standards of medical Care in diabetes-2022. Diabetes Care *45*, S125–S143.

50. American Diabetes Association (2021). 9. Pharmacologic approaches to glycemic treatment: standards of medical Care in diabetes-2021. Diabetes Care *44*, S111–S124.

51. Pirola, L., Balcerczyk, A., Okabe, J., and El-Osta, A. (2010). Epigenetic phenomena linked to diabetic complications. Nat. Rev. Endocrinol. *6*, 665–675.

52. Brown, A., Reynolds, L.R., and Bruemmer, D. (2010). Intensive glycemic control and cardiovascular disease: an update. Nat. Rev. Cardiol. *7*, 369–375.

53. Paneni, F., Mocharla, P., Akhmedov, A., Costantino, S., Osto, E., Volpe, M., Lüscher, T.F., and Cosentino, F. (2012). Gene silencing of the mitochondrial adaptor p66(Shc) suppresses vascular hyperglycemic memory in diabetes. Circ. Res. *111*, 278–289.

54. Yancy, C.W., Jessup, M., Bozkurt, B., Butler, J., Casey, D.E., Jr., Drazner, M.H., Fonarow, G.C., Geraci, S.A., Horwich, T., Januzzi, J.L., et al. (2013). 2013 ACCF/AHA guideline for the management of heart failure: executive summary: a report of the American College of Cardiology Foundation/American Heart Association Task Force on practice guidelines. Circulation *128*, 1810–1852.

55. Meagher, P., Adam, M., Civitarese, R., Bugyei-Twum, A., and Connelly, K.A. (2018). Heart failure with preserved ejection fraction in diabetes: mechanisms and management. Can. J. Cardiol. *34*, 632–643.

56. Ren, X.P., Wu, J., Wang, X., Sartor, M.A., Jones, K., Qian, J., Nicolaou, P., Pritchard, T.J., and Fan, G.C. (2009). MicroRNA-320 is involved in the regulation of cardiac ischemia/reperfusion injury by targeting heat-shock protein 20. Circulation *119*, 2357–2366.

57. He, M., Wang, J., Yin, Z., Zhao, Y., Hou, H., Fan, J., Li, H., Wen, Z., Tang, J., Wang, Y., et al. (2019). MiR-320a induces diabetic nephropathy via inhibiting MafB. Aging *11*, 3055–3079.

58. Yin, Z., Zhao, Y., Li, H., Yan, M., Zhou, L., Chen, C., and Wang, D.W. (2016). miR-320a mediates doxorubicin-induced cardiotoxicity by targeting VEGF signal pathway. Aging *8*, 192–207.

59. Veronese, G., Ammirati, E., Chen, C., Klingel, K., Suzuki, M., Okumura, T., Maisch, B., Zuo, H., Ni, L., Jiang, J., et al. (2021). Management perspectives from the 2019 Wuhan international workshop on fulminant myocarditis. Int. J. Cardiol. *324*, 131–138.

60. Fuji, T., Umeda, Y., Nyuya, A., Taniguchi, F., Kawai, T., Yasui, K., Toshima, T., Yoshida, K., Fujiwara, T., Goel, A., and Nagasaka, T. (2019). Detection of circulating microRNAs with Ago2 complexes to monitor the tumor dynamics of colorectal cancer patients during chemotherapy. Int. J. Cancer *144*, 2169–2180.

61. Turchinovich, A., Weiz, L., and Burwinkel, B. (2013). Isolation of circulating microRNA associated with RNA-binding protein. Methods Mol. Biol. *1024*, 97–107.

62. Squadrito, M.L., Baer, C., Burdet, F., Maderna, C., Gilfillan, G.D., Lyle, R., Ibberson, M., and De Palma, M. (2014). Endogenous RNAs modulate microRNA sorting to exosomes and transfer to acceptor cells. Cell Rep. *8*, 1432–1446.

63. Melo, S.A., Sugimoto, H., O'Connell, J.T., Kato, N., Villanueva, A., Vidal, A., Qiu, L., Vitkin, E., Perelman, L.T., Melo, C.A., et al. (2014). Cancer exosomes perform cell-independent microRNA biogenesis and promote tumorigenesis. Cancer Cell *26*, 707–721.

64. Qiao, L., Hu, S., Liu, S., Zhang, H., Ma, H., Huang, K., Li, Z., Su, T., Vandergriff, A., Tang, J., et al. (2019). microRNA-21-5p dysregulation in exosomes derived from heart failure patients impairs regenerative potential. J. Clin. Invest. *129*, 2237–2250.

65. Bang, C., Batkai, S., Dangwal, S., Gupta, S.K., Foinquinos, A., Holzmann, A., Just, A., Remke, J., Zimmer, K., Zeug, A., et al. (2014). Cardiac fibroblast-derived microRNA passenger strand-enriched exosomes mediate cardiomyocyte hypertrophy. J. Clin. Invest. *124*, 2136–2146.

66. Datta, R., Bansal, T., Rana, S., Datta, K., Datta Chaudhuri, R., Chawla-Sarkar, M., and Sarkar, S. (2017). Myocyte-Derived Hsp90 modulates collagen upregulation via biphasic activation of STAT-3 in fibroblasts during cardiac hypertrophy. Mol. Cell Biol. *37*, e00611-16.

67. Ye, X., Qi, J., Wu, Y., Yu, D., Xu, P., Li, S., Zhu, S., Wu, Q., Ren, G., and Li, D. (2015). Comparison of PEGylated FGF-21 with insulin glargine for long-lasting hypoglycaemic effect in db/db mice. Diabetes Metab. *41*, 82–90.

68. Xiao, X., Li, J., and Samulski, R.J. (1998). Production of high-titer recombinant adeno-associated virus vectors in the absence of helper adenovirus. J. Virol. *72*, 2224–2232.

69. Weng, S., Zhao, Y., Yu, C., Wang, X., Xiao, X., Han, L., Zhang, K., Wang, J., and Yang, G. (2021). Construction of a rAAV-SaCas9 system expressing eGFP and its application to improve muscle mass. Biotechnol. Lett. *43*, 2111–2129.

70. Tiedje, C., Ronkina, N., Tehrani, M., Dhamija, S., Laass, K., Holtmann, H., Kotlyarov, A., and Gaestel, M. (2012). The p38/MK2-driven exchange between tristetraprolin and HuR regulates AU-rich element-dependent translation. PLoS Genet. *8*, e1002977.

71. Syed, F., Diwan, A., and Hahn, H.S. (2005). Murine echocardiography: a practical approach for phenotyping genetically manipulated and surgically modeled mice. J. Am. Soc. Echocardiogr. *18*, 982–990.

72. Schaefer, A., Klein, G., Brand, B., Lippolt, P., Drexler, H., and Meyer, G.P. (2003). Evaluation of left ventricular diastolic function by pulsed Doppler tissue imaging in mice. J. Am. Soc. Echocardiogr. *16*, 1144–1149.

73. Schmidt, A.G., Gerst, M., Zhai, J., Carr, A.N., Pater, L., Kranias, E.G., and Hoit, B.D. (2002). Evaluation of left ventricular diastolic function from spectral and color M-mode Doppler in genetically altered mice. J. Am. Soc. Echocardiogr. *15*, 1065–1073.